

A Multi-Year Photopolarimetric Study of the Semi-Regular Variable V CVn and Identification of Analogue Sources

H. Neilson¹, N. Steenken², J. Simpson³, R. Ignace⁴, M. Shrestha^{5,6}, C. Erba⁴, and G. Henson⁴

¹ Department of Physics & Physical Oceanography, Memorial University of Newfoundland & Labrador, St. John's, NL, Canada A1C 5S7

e-mail: hneilson@mun.ca

² Sternwarte Freimann, 80939 Munich, Germany

³ Parton, Scotland, UK

⁴ Department of Physics & Astronomy, East Tennessee State University, Johnson City, TN 37614, USA

⁵ Astrophysics Research Institute, Liverpool John Moores University, Liverpool Science Park, 146 Brownlow Hill, Liverpool, L3 5RF, UK

⁶ Steward Observatory, University of Arizona, 933 North Cherry Avenue, Tucson, AZ 85721-0065, USA

ABSTRACT

The semi-regular variable star V Canum Venaticorum (V CVn) is well-known for its unusual linear polarization position angle (PA). Decades of observing V CVn reveal a nearly constant PA spanning hundreds of pulsation cycles. This phenomenon has persisted through variability that has ranged by 2 magnitudes in optical brightness and through variability in the polarization amplitude over 0.3% and 6.9%. Additionally, the polarization fraction of V CVn varies inversely with brightness.

This paper presents polarization measurements obtained over three pulsation cycles. We find that the polarization maximum does not always occur precisely at the same time as the brightness minimum. Instead, we observe a small lead or lag in relation to the brightness minimum, spanning a period of a few days up to three weeks. Furthermore, the PA sometimes exhibits a non-negligible rotation, especially at lower polarization levels.

To elucidate the unusual optical behavior of V CVn, we present a list of literature sources that also exhibit polarization variability with a roughly fixed PA. We find this correlation occurs in stars with high tangential space velocities, i.e., “runaway” stars, suggesting that the long-term constant PA is related to how the circumstellar gas is shaped by the star’s high-speed motion through the interstellar medium.

Key words. Polarization – Stars: V CVn (HD 115898), L₂ Pup, UZ Ari, AK Peg, RX Boo, Z UMa – Mass-loss, Circumstellar matter, AGB, post-AGB

1. Introduction

Semi-regular variable stars (SRVs) are intriguing objects. They are evolved, pulsating red giant stars that reflect the future of our own Sun. SRVs are distinguished from Mira-type stars by their smaller brightness amplitude that is less than 2.5 mag(V). In particular, SRV stars of type ‘a’ (SRa) show an identifiable and sustainable primary pulsation period and in many cases secondary pulsation periods.

SRV stars, which are bright and so have been observed for centuries, are recognized as important standard candles that also follow a number of period-luminosity relations (Trabucchi et al. 2017; Lebzelter et al. 2019). This correspondence contributes to our understanding of their evolution, and makes SRVs valuable to extragalactic and cosmological studies. Even after so many observations and studies SRVs continue to present a number of questions, including the role of convection, stellar and circumstellar magnetic fields, atmospheric dynamics, winds, along with how these stars interact with their circumstellar medium (Kerschbaum & Hron 1992; Kudashkina 2019).

One of the more surprising questions arises from linear polarization measurements of some SRV stars. Kruszewski et al. (1968) and Shawl (1975a,b) presented early polarization measurements for V CVn (HD 115898). This M4e-M6eIIIa late

AGB star has a highly variable polarization and is located at a distance of 501 pc (Gaia Collaboration 2020). Linear polarization measurements of unresolved sources can measure deviations from circular symmetry as projected onto the sky. Thus, the detection of linear polarization from a star may indicate an asymmetry that due to the presence of convection, wind bow shocks, or disks (Shrestha et al. 2021).

Kruszewski et al. (1968) presented time-domain polarization measurements of V CVn showing that the polarization fraction changes over the approximate 194 day primary pulsation period, while the position angle remains constant. What is more curious is that the polarization fraction appears to be anti-correlated to the brightness of the star: when the star is brightest, the polarization is at a minimum; and when the star is dimmest, the polarization is at a maximum. This surprising behaviour was confirmed to be a function of wavelength by Magalhaes et al. (1986a,b). While still unexplained, this phenomenon is not unique to V CVn.

Kruszewski et al. (1968) identified similar polarization variability in the star L₂ Puppis. This result added to the challenge of understanding these two stars, but resolved polarimetric observations provided information about the circumstellar structure of the L₂ Pup system. Kervella et al. (2015) used VLT

SPHERE/ZIMPOL polarimetric observations to discover the presence of a circumstellar disk. This disk is remarkable as its asymmetry projected on the sky explains the constant position angle of the unresolved linear polarization, but not the variation of the polarization itself.

Neilson et al. (2014) reviewed time-domain polarization measurements for V CVn, and confirmed the periodic variability of the polarization while the position angle stays approximately constant. They also confirmed that the maximum value of the polarization appeared to correspond to minimum brightness, and the minimum polarization to maximum brightness. They suggested that the polarization and position angle time-domain observations could be explained by a pulsation-driven, spherically symmetric dusty wind that interacts with an asymmetric stellar wind bow shock. The presence of a constant bow shock could explain the constant position angle. When the star approaches maximum brightness, it also approaches maximum radius and minimum effective temperature. Thus, dust will form in the spherically symmetric outflow, and that dust will be more likely to interact with scattering photons from the star. This will cause the polarization to decrease to a minimum. Conversely, as the shell expands, the density decreases and the shell will interact with the bow shock, creating a highly asymmetric system, and resulting in a maximum polarization value, as shown by Shrestha et al. (2021).

An alternative model was proposed by Safonov et al. (2019) based on differential speckle polarimetric observations of V CVn. They introduced the idea of scattering arcs or reflection nebulae in the circumstellar envelope of the star; hereafter we refer to these as simply "blobs". In their model, some blobs are in the background, and some are in the foreground of the system. In this geometry, the authors argued that the polarization variability could be explained if the star undergoes a form of non-radial variability of its brightness which could be either dipolar pulsation or rotational variation, such that when the star appears brightest, an observer behind the star would see V CVn at maximum brightness, and vice versa. Because one blob appears to be behind the star, when we see V CVn at minimum light, the distant blob will see intercept photons from the star at maximum brightness on the far side, and thus there will be more backscattered photons, hence the polarization will be greatest.

The polarization variability of V CVn can thus be explained by both of these scenarios, but they each depend on the circumstellar medium (CSM) structures of V CVn and L₂ Pup. Understanding the CSM of these stars offers important insights into how evolved semi-regular variable stars lose mass, and potentially connects to their future evolution into planetary nebulae. In a collaboration between professional and amateur astronomers, we consider here new time-domain polarization observations of V CVn (led by co-authors Steenken and Simpson) that offer new tests of the two models mentioned. This is an especially valuable collaboration because V CVn is too bright for most large telescopes. Therefore it was advantageous to perform this investigation in cooperation with amateur astronomers. In Section 2, we discuss the tools and methods used to obtain new observations of V CVn. In Section 3, we compare the polarimetric observations with the visual brightness of the star. Section 4 then presents a review of potential analogues to V CVn and L₂ Pup, and we suggest that these stars are actually the prototypes of a class of polarimetric semi-regular variable stars ("V CVn type" stars). We discuss the various CSM and polarizations models for V CVn to discern if and how these new observations might provide new insights into this system. Finally, Section 5 presents our conclusions and suggestions for future observations.

2. Observations and Data Reduction

Optical polarization observations and photometry of V CVn were carried out independently by two of the co-authors (Steenken and Simpson; hereafter "observers") operating Schmidt-Cassegrain Telescopes (SCT). The observers are located in Munich/Germany (Steenken, Ob1) and in Parton/Scotland (Simpson, Ob2). Both telescopes have Dual-Beam-Polarimeters with V-band filters and cooled CCD cameras mounted at the Cassegrain focus. Customary SCTs were used, with OB1 having a focal length of 2800 mm and aperture of 280 mm, and OB2 using a two different SCTs with focal lengths of 1500 and 2000 mm and apertures of 150 and 200 mm (Ob2) on a German equatorial mount. Object centering and autoguiding was achieved with separate guide scopes and guiding cameras.

Both polarimeters were built and calibrated in 2018-2019 to measure the linear optical polarization (P) of stars brighter than 9 mag, with an error of $\pm 0.1\%$ polarization and ± 5 degrees of polarization position angle (PA) in the relevant polarization range of V CVn in the past i.e. 0.3% - 6.9%. An achromatic Half-Wave-Plate (HWP) was manually rotated into the positions 0, 22.5, 45 and 67.5 degrees to rotate the polarization plane 0, 45, 90 and 135 degrees. The 0 degree position is aligned with the celestial North direction. The instrumental 0 deg position has been nominally aligned with the celestial NS reference and offsets from this are checked during each observing session, using measurements obtained either by plate solving a stacked measurement image and/or by disabling tracking so as to generate an EW trace on measured images and therefore a NS reference. These offsets are removed during data processing. Calibration, later performed, uses high polarisation standards to correct instrumental position angle offsets arising from any half-wave plate/Wollaston prism misalignments. A Wollaston prism splits the star into a parallel and a perpendicular beam. The beams are passed through a V-band filter and focused onto a CCD detector of 1392×1040 pixels for a cooled 16-bit Astro camera. The optical design is shown in Fig. 1.

The images were captured and analyzed with standard image capturing and photometry software (for Ob1: AstroArt 6¹ and for Ob2: AstroImageJ²). The exposure times vary from 2 to 15 seconds depending on the star brightness, weather conditions and telescope. For one observation, 40 to 100 images in each rotation position of the HWP were exposed. Batch processing was used for the dark field correction, stellar alignment, and photometry of the parallel and perpendicular stellar images. Aperture radii selection, based on the image's full width at half maximum [FWHM] – typically 1.5-2 times FWHM for the signal and 3 resp. 5 times FWHM respectively for inner/outer annuli for sky background evaluation – provided a flux measurement that is robust against seeing variations, giving confidence in the method even when the object images were slightly distorted. Signal-to-noise ratios (SNR) of over 400 of each image taken as calculated by the photometry software were achieved, subject to atmospheric conditions. Fig. 2 shows an example of an image made by Ob 1.

Fluxes of parallel $f_{par,i}$ and perpendicular beams $f_{perp,i}$ were measured for every image i with the photometry software. Polarization (P), including correction for bias, and Position Angle (PA) were calculated as described in Clarke (2010). For the error analysis, the study by Patat & Romaniello (2006) was used.

¹ www.msb-astroart.com

² www.astro.louisville.edu

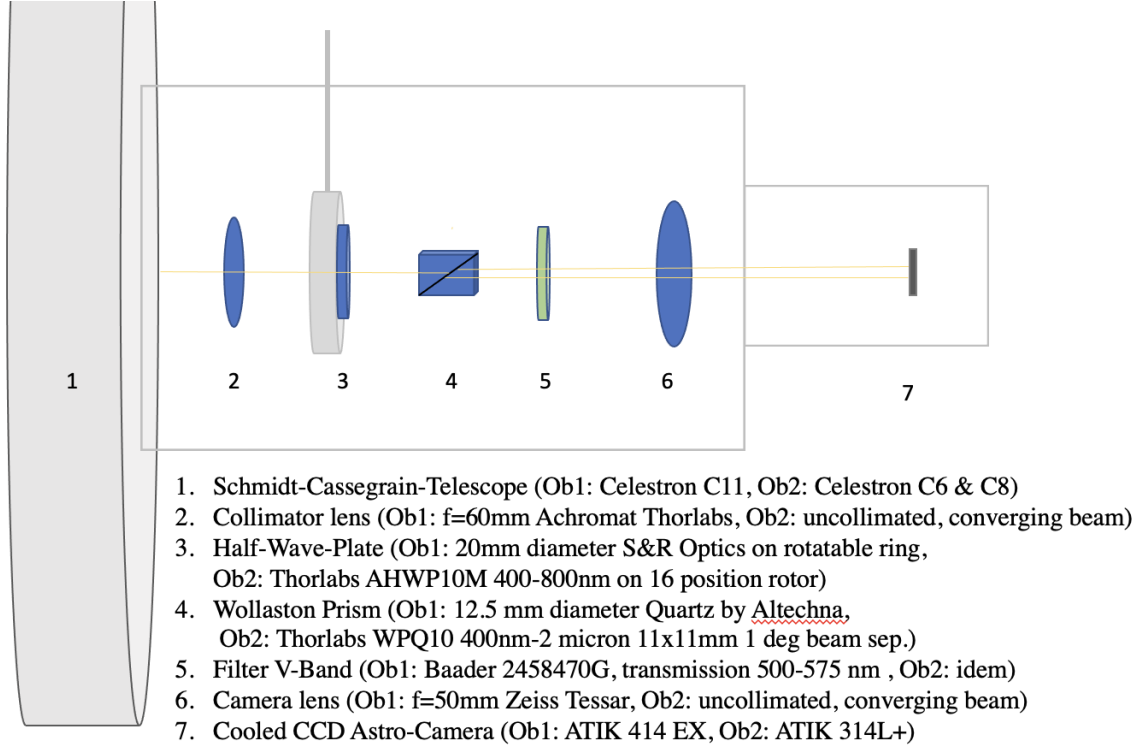


Fig. 1. Optical design of the dual-beam-polarimeter, with components along the optical path identified and labeled.

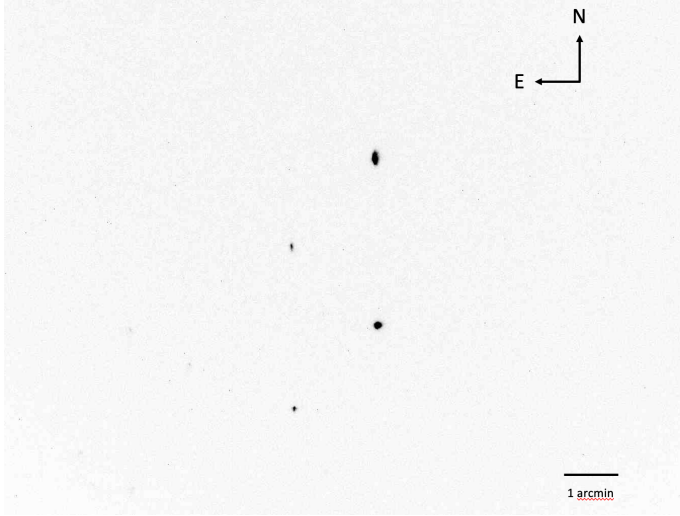


Fig. 2. An example of one image of V CVn split into parallel (bright star at top) and perpendicular beams (bright star at bottom) from 2022-07-03 at 0 degree rotation position. The star left below V CVn is BD+46 1863.

To calculate the measured Stokes Q_m and U_m parameters, parallel and perpendicular flux measurements are combined in the following way, for angle positions θ :

$$N_\theta = \frac{\sum f_{par_i} - \sum f_{perp_i}}{\sum f_{par_i} + \sum f_{perp_i}}, \quad (1)$$

$$Q_m = \frac{1}{2}(N_0 - N_{45}) \text{ and} \quad (2)$$

$$U_m = \frac{1}{2}(N_{22.5} - N_{67.5}) \quad (3)$$

Table 1. Unpolarized stars used as standards, and their polarization according to Schmidt et al. (1992)

Star	$mag(V)$	P (%)	σ_P (%)	Observer
β Cas	2.3	0.037	0.024	1,2
θ UMa	3.2	0.037	0.014	1,2
β UMa	2.4	0.009	0.019	2
HD 21447	5.1	0.051	0.020	1

where N_θ is the fractional photon count between parallel and perpendicular beams at the specified angle of the Half-Wave-Plate.

Any optical design of a polarimeter has to deal with instrumental polarization caused by the telescope or the optical components in the polarimeter, including the filter. To remove the instrumental polarization effects, the Stokes parameters of unpolarized stars in Table 1 were measured as zero-point offsets and calibrated Stokes parameters calculated using:

$$Q_{cal} = Q_m - Q_0, \text{ and} \quad (4)$$

$$U_{cal} = U_m - U_0 \quad (5)$$

Calibration standard high polarization stars like ϕ Cas and 2H Cam were measured in agreement to the published values of Hsu & Breger (1982) as shown in Table 2. Both the instrumental set-ups and zero-point offsets were kept unchanged during the observing seasons from January until September to ensure comparable results. Calibration stars were observed each season to determine the stability and the reliability of the polarization position angle.

V-band photometry of V CVn was obtained directly before or after the polarimetric measurements with nearby comparison stars. Ob1 selected nearby star HD 116957, with $mag(V) = 5.87$,

Table 2. Highly polarized stars measurements and comparison to reference

Star	JD	P_{cal}	PA_{cal}	Ob
ϕ Cas	2459077	3.30%	98.8	1
ϕ Cas	2459280	3.42%	95.7	1
ϕ Cas	2459448	3.32%	95.6	1
ϕ Cas	2459452	3.12%	96.6	1
ϕ Cas	2459599	3.35%	93.8	1
ϕ Cas	2459599	3.34%	92.7	1
ϕ Cas	2459622	3.29%	92.8	1
ϕ Cas	2459808	3.44%	96.0	1
ϕ Cas	Average	3.32%	95.3	1
<hr/>				
ϕ Cas	2459287	3.41%	93.3	2
ϕ Cas	2459287	3.24%	92.0	2
ϕ Cas	2459314	3.44%	92.7	2
ϕ Cas	Average	3.36%	92.7	2
ϕ Cas	Hsu & Breger (1982)	3.34%	92.3	
<hr/>				
2H Cam	2459319	3.37%	115.2	2
2H Cam	2459543	3.53%	115.0	2
2H Cam	Average	3.45%	115.1	2
2H Cam	Hsu & Breger (1982)	3.49%	116.6	

as comparison. Ob2 used an ensemble of the four AASVO comparison stars³.

The measured polarization is composed of the intrinsic polarization of V CVn and the interstellar polarization.

The star BD+46 1863 is located only about 2 arcmin southwest of V CVn at a distance of about 1670 pc and was used estimate the interstellar polarization. The measurements performed on the nearby stars TYC 3460-1345-1 and TYC 3460-2045-1 gave values of polarization between 0 and 0.5%. However, due to the high measurement uncertainties, these measurements were not used. The estimate is as shown in table 3 and is the basis for the calculation of the intrinsic polarization of V CVn.

Table 3. Estimate of interstellar polarization based on nearby star BD+46 1863

P_{is}	PA_{is}	Q_{is}	U_{is}	σ_Q	σ_U
0.34%	123	-0.14%	-0.31%	0.010%	0.009%

Intrinsic Stokes Q_{intr} and U_{intr} parameters were calculated according to:

$$Q_{intr} = Q_{cal} - Q_{is}, \text{ and} \quad (6)$$

$$U_{intr} = U_{cal} - U_{is} \quad (7)$$

Intrinsic Polarization P_{intr} and intrinsic polarization angle PA_{intr} according to:

$$P_{intr} = \sqrt{Q_{intr}^2 + U_{intr}^2}, \text{ and} \quad (8)$$

$$PA_{intr} = \frac{1}{2} \tan^{-1} \left(\frac{U_{intr}}{Q_{intr}} \right). \quad (9)$$

The standard error of the mean values of Stokes Q, U were calculated according to Clarke (2010) using the student-t distri-

³ Chart X28069ADU, AASVO Variable Star Database

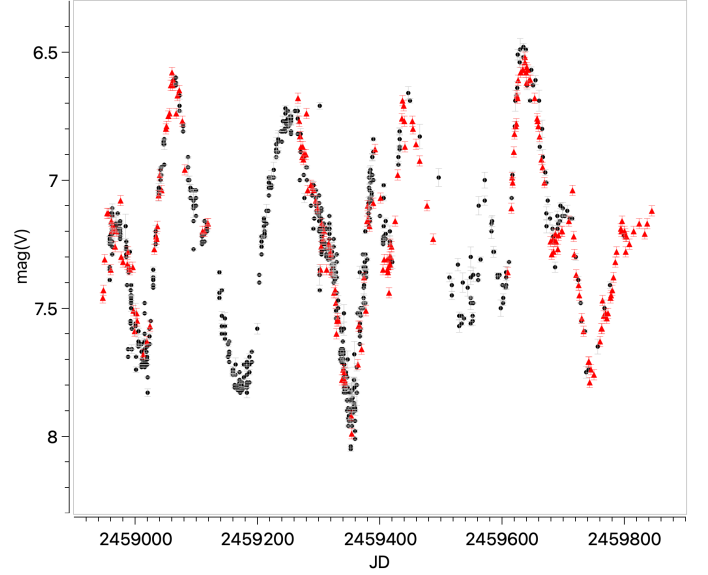


Fig. 3. The V-band light curve of V CVn from 2020-2022. The red triangles are the photometry measurements provided by Ob1 and Ob2. The grey dots are for AASVO data (CCD measurements only). The three pulsation cycles covered by polarization measurements in this study in red, namely at the left pulsation cycle 1/2020 in the middle 1/2021 and at the right cycle 1/2022. It can be seen that the data from AASVO agrees well with the data measured by Ob1 and Ob2. Pulsation cycle 1/2021 showed the lowest brightness of all minima considered.

bution for 95% confidence limits. Errors of P and PA and were calculated as follows:

$$\sigma_P = \frac{\sqrt{Q^2 \sigma_Q^2 + U^2 \sigma_U^2}}{P} \quad (10)$$

$$\sigma_{PA} = \frac{\sqrt{Q^2 \sigma_U^2 + U^2 \sigma_Q^2}}{2P^2} \quad (11)$$

In the data reduction process polarization has been de-biased using the Wardle & Kronberg (1974) formulation:

$$P_{debias} = \sqrt{P_{cal}^2 - \sigma_P^2} \quad (12)$$

A total of 227 measurements were taken on 51 nights in 2020, 89 nights in 2021, and 87 nights in 2022, with a table of measurements in Appendix B⁴. During this span of time, V CVn went through 5 pulsation cycles, as shown in Fig. 3. The polarization measurements covered the first pulsation cycle in 2020, 2021 and 2022 (hereafter 1/2020, 1/2021 and 1/2022).

3. Results

The relationship between intrinsic polarization and brightness over the course of all three pulsation cycles is shown in Fig. 4. The polarization in the V-Band is highly variable, and is generally anti-correlated with brightness. The larger polarizations were measured around brightness minima, and are consistent with earlier studies by Serkowski & Shawl (2001) and Davidson et al. (2014).

⁴ All raw data can be obtained from <https://zenodo.org/record/7997101>

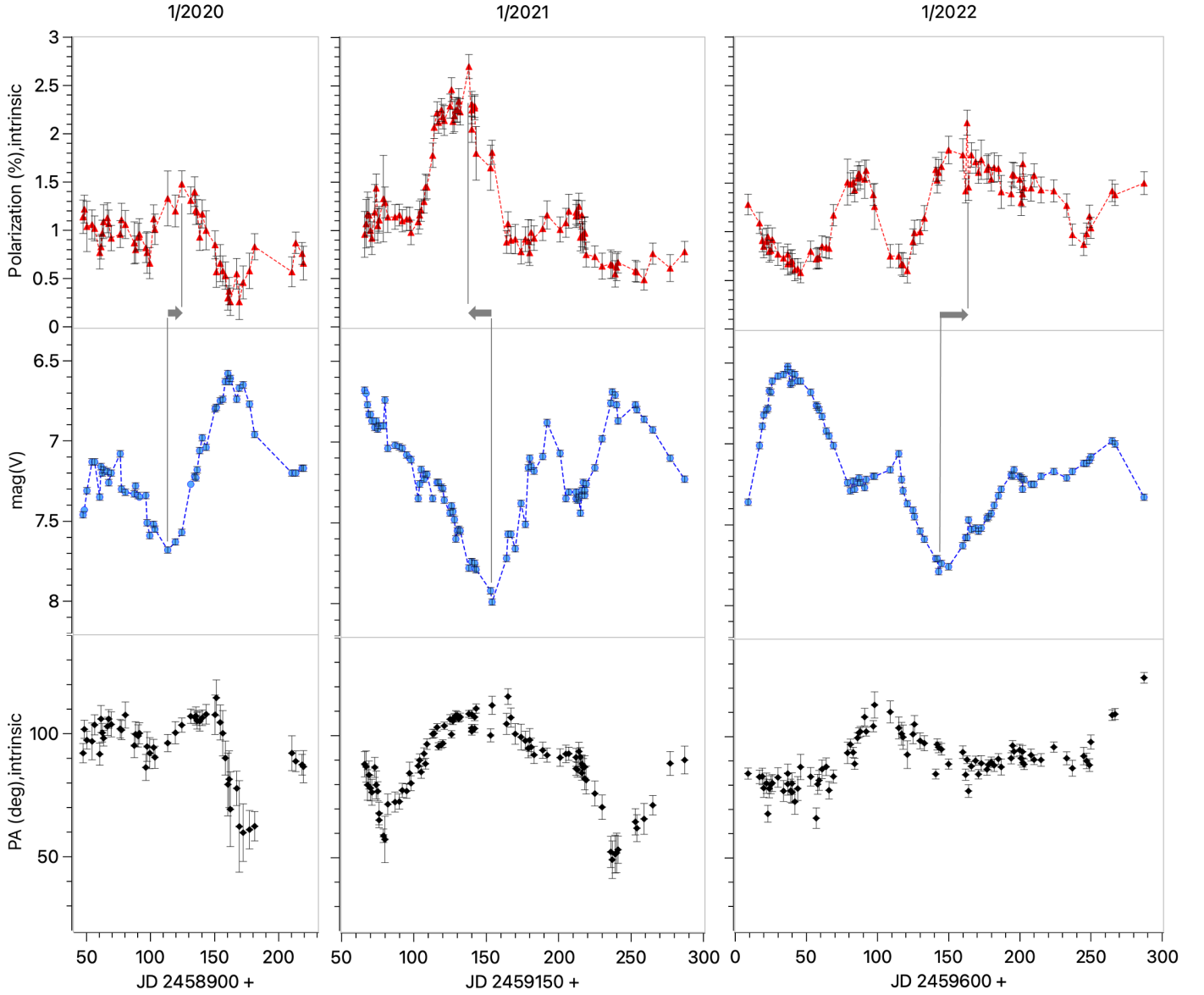


Fig. 4. Photopolarimetry of the observed pulsation cycles. Intrinsic polarization curves in red are shown in the upper row. The light curves in blue are shown in the middle row. The intrinsic position angle (PA) is shown in the lower row as black. In all three pulsation cycles polarization and photometry are generally anti-correlated, especially true around times of brightness maxima and minima. However, the curves are not exactly anti-correlated as indicated by the grey arrows. A phase shift between polarization and total light is most clearly visible around the brightness minimum of pulsation cycle 1/2021, but also seen in pulsation cycles 1/2020 and 1/2022. Comparison between the 3 cycles reveals that the polarization curve can either lead or lag the light curve. The intrinsic PA ranges generally within 80 – 120 degrees, except when the star is brighter than 7 mag(V) and/or the polarization drops significantly below 0.7%. At such times, the PA can drop below 50 degrees.

Thanks to the high cadence of measurements covering three pulsation cycles, the temporal relationship between the star’s light curve and polarization can be analyzed in more detail. Pulsation cycle 1/2021 showed the strongest obscuration associated with the highest measured intrinsic polarization of all three observed pulsation cycles. Of particular interest is the observation that the maximum polarization does not occur exactly at the time of the minimum brightness of V CVn. We observe that in the three cycles that the polarization maximum can lead the brightness minimum by several weeks as well as lag it. Especially in cycle 1/2021 polarization led by about 16 days and in cycle 1/2022 polarization lagged again by about 20 days. This lead/lag phenomenon was observed around brightness minima and is indicated by a grey arrows in Fig. 4. The pulsation cycle 1/2020 is shown in the left column of the figures. Polarisation maximum

of 1.47% was reached at JD 2459024. The brightness at 7.68 mag(V) minimum occurred 11 days (JD 2459013) before. Polarization was lagging the light curve. In the pulsation cycle 1/2021 (middle column) polarization was leading the light curve. The maximum of intrinsic polarization of 2.70% was measured at JD 2459338 16 days before the first minimum of the light curve which occurred at JD 2459354 and reached 7.99 mag(V). In this pulsation cycle, the star darkened significantly more and reached much higher polarization values than in the other two cycles. In the pulsation cycle 1/2022 (right column) polarization was lagging again the light curve. Second light minimum occurred on JD 2459743 at 7.79 mag(V) which was followed by the polarization maximum of 2.11% on JD 2459763 20 days later. Due to the irregular course of the light curve and the daily variations in brightness and polarization, an exact determination of the shift is

not possible. Polarization showed strong variations while going through the maximum. There are indications that phase shifts between the curves may occur when the polarization changes significantly within a few weeks. During periods of little change in brightness, there appears to be little correlation between the curves. The position angle PA stays generally within a range of 80 - 120 degrees, except when the intrinsic polarization drops below 0.7%.

4. Discussion

4.1. A New Class of V CVn-type Stars

The *Combined General Catalog of Variable Stars* (Samus et al. 2004) lists 348 SRa and 1201 SRb stars, yet polarimetric measurements have only been published for a few of them. As a consequence, it is unknown whether significant variation of the polarization during a pulsation cycle of more than 1% is typical or exceptional for semi-regular variables.

While V CVn is not the only semi-regular evolved star with significant variable polarization, it by far has the greatest number of polarization measurements obtained since the 1960s. Table A.1 (A) lists the basic stellar parameters of five other semi-regular stars that show polarimetric behavior similar to V CVn itself. The following list summarizes their observed properties:

- UZ Ari (IRC +20052) appears similar to V CVn in many respects. It is situated at high galactic latitude (-31 deg) at a similar distance (539 pc), and has a tangential velocity of 59 km/sec. The period of UZ Ari is 163 days, about 30 days shorter than of V CVn. UZ Ari has a spectral class of M8, with an apparent brightness that is significantly lower than V CVn, and varies between 11.8 and 12.6 mag(V). Baug et al. (2014) were able to measure the diameter of the star in K-band during three lunar occultations. They found values of $4.5 - 6.0 \pm 0.5$ mas without a correlation to phase. The few published polarization measurements in the V-band vary between 2 and 3.5%, with a decade long stable PA around 130 deg (Kruszewski & Coyne 1976; Baug et al. 2014). If future polarization measurements of UZ Ari confirm the stable range of PA, then the physical origin of the asymmetry could be the same as in V CVn.
- AK Peg has a very similar period of variability and spectral type to V CVn. At its distance of 1329 pc, the star ranges in brightness between 8.6 - 10.2 mag(V). The few polarization measurements published by Serkowski & Shawl (2001) indicated polarization values between 1.5 and 3.4%, a fairly large intrinsic level of polarimetric variability similar to UZ Ari.
- RX Boo has variability that is classified as an SRb, with a distance of 156 pc. Using the Infrared Optical Array Imaging Interferometer (IOTA), Ragland et al. (2006) measured a stellar diameter of 17.5 mas in H-Band that showed no asymmetry. Unfortunately, only a few older polarization measurements are available for this star (Vartanyan 1968), with values ranging from 0.4 to 1.9%. The change in polarization is comparable to UZ Ari and AK Peg.
- Z UMa is an SRb star at a distance of 296 pc. Dyck & Jennings (1971) published polarization measurements ranging between 0.2 and 1.8%. Measurements at 5 epochs by Ob1 in 2021 (Fig. 5) confirmed variable polarization from 0.13 to 1.0%, showing an anti-correlation with brightness. Again, the amplitude of variable polarization is comparable to the previous three objects.
- L₂ Pup is an SRb star on the southern hemisphere. The polarization measurements of Magalhaes et al. (1986b) reveal

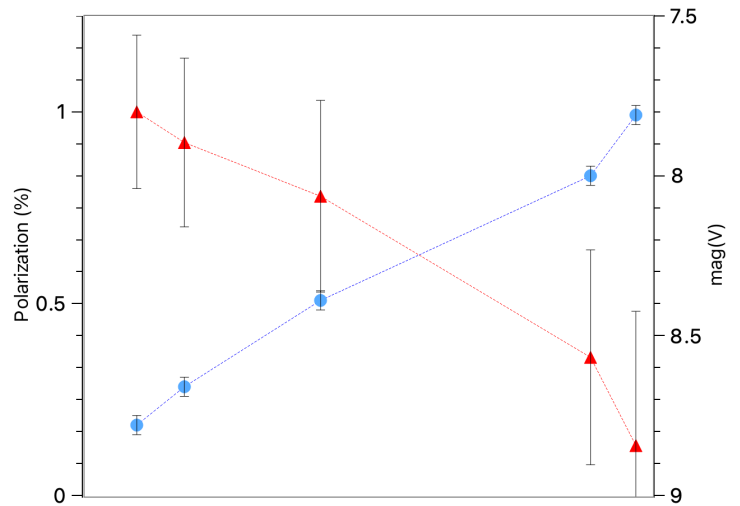


Fig. 5. Polarization measurements (red triangles) and photometry (blue dots) of Z UMa in 2021 (Ob1). Five epochs of photopolarimetric measurements were obtained. The data give indications of an anti-correlation between the measured polarization and brightness.

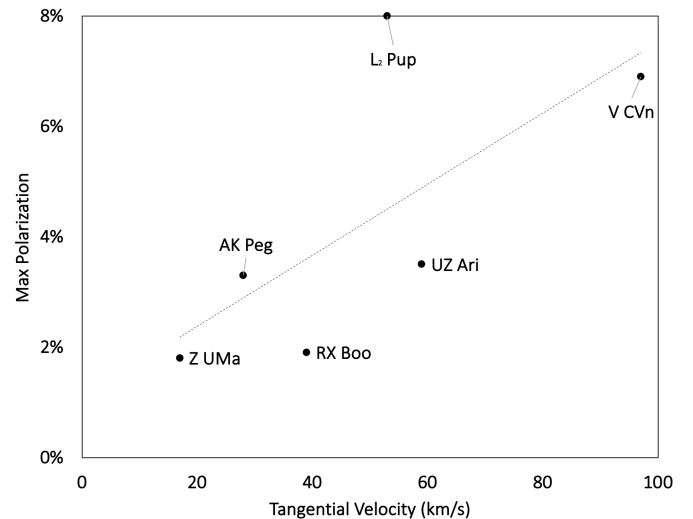


Fig. 6. Maximum polarization vs. tangential velocity of the stars in Table A.1, indicating an higher maximum polarization with increased tangential velocity.

a high level of polarization variability between 0 and 8%, accompanied by a steady PA of 165-180 degrees. If the few historical polarization V-band measurements are compared with photometric data from the AASVO, the polarization appears anti-correlated with brightness level. This level of variable polarization is considerably larger than the four preceding stars, but is comparable to V CVn.

Due to a distance of only 56 pc, and the superior imaging performance of VLT SPHERE/ZIMPOL, it has been possible to detect a dust disk responsible for the asymmetry of L₂ Pup (Kervella et al. 2015). For the other stars listed above, the reasons for the asymmetries remain unclear. None of these stars are located in the galactic plane, with its higher interstellar density, but some of them show high tangential or radial velocities.

In Fig. 6, we see hints of a relationship between the tangential velocity and the observed maximum polarization. Stars with significant tangential velocities and slow winds, such as

those from cool, evolved stars, would be expected to host a bow shock along the plane of the sky. That bow shock, if unresolved, would create a significant asymmetry on the plane of the sky with an associated polarization signature (Shrestha et al. 2021). The amount of polarization would depend on both the shape and density of the bow shock, along with the properties of the stellar wind. Shrestha et al. (2021) showed that polarization is a function of the type of dust in the bow shock, the density of the local interstellar medium, and the wind properties of the stars in question, so the apparent correlation of Figure 6 could be consistent with the model proposed by Neilson et al. (2014). The polarization would be variable if, during the phase where V CVn is brightest, the star ejects a dusty shell whose density is sufficient to wash out the bow shock signal and make the system appear more symmetric (Shrestha et al. 2021).

Safonov et al. (2019) argued that V CVn cannot have a bow shock, due to a low ISM density expected from its high galactic latitude. However, the star is located only a few arcmin away from a molecular cloud discovered by Reach et al. (1994). The molecular cloud G107.4 +70.9 is one of the densest clouds in that region, and lies roughly at the same distance as V CVn, according to a study from Gladders et al. (1998). It is plausible that the interstellar density near the fast moving V CVn could be large enough to allow the formation of a bow shock.

4.2. Possible models of the polarimetric variability

The polarimetric variability of V CVn is surprising and counter-intuitive. When the star reaches maximum light, the polarization approaches a minimum, and vice-versa. One might expect that if the source of the polarization were constant – which would yield a constant position angle – then at maximum light, the number of polarized photons would also be at a maximum. However, since the polarization is a normalized quantity, one would find that the polarization is also constant. Satisfying the observations requires either of the following scenarios:

1. The source of the polarization interacts with a different number of photons relative to what the observer sees (Safonov et al. 2019); or
2. The source of the polarization changes, yet maintains the same deviation of symmetry on the sky (Neilson et al. 2014).

The results of this work impose an additional requirement that a viable model should explain observed time differences between the polarization maximum and the light minimum.

If we consider the first option, Safonov et al. (2019) suggest that one of the dusty “blobs” is behind the star relative to the observer (c.f., Sec. 1). They suggest that if the light variation is not due to radial pulsation, and instead is some type of dipolar variability or rotational variability, then when the observer measures minimum light, the other side of the star appears at maximum light – hence the blob “sees” the greatest number of polarizing photons that get backscattered to the observer. This model is intriguing, but requires the stellar variability to be asymmetric and non-radial. The pulsation amplitude of V CVn is about 2 mag(V), and there are no known stars that pulsate with this amplitude non-radially. If this were a rotational phenomena, combining a period of about ≈ 194 d with an assumed stellar radius of order $100 R_{\odot}$ implies the rotation rate is about 25 km s^{-1} , and is the same order as the critical rotation rate for the star.

An additional challenge for this model is the apparent lead and lag time between polarization and flux. If the issue was only that the polarization maximum lagged behind the luminosity, one might explain it as a light-time delay of $t_d = 22d_b/c$, where d_b

is the distance between the star and blob. Safonov et al. (2019) reported a radius of the blobs around V CVn of 35 ± 1 mas. Using the latest distance data from Gaia Collaboration (2020) of 501 pc, this results in a distance of the bipolar cloud of 17.5 AU. The time delay caused by the light travelling between the assumed bipolar cloud and the star is then 2.5 hr, and thus by far not enough to explain the observed time difference in our observational data between the light and polarization curves of up to two weeks.

Neilson et al. (2014) suggest that the variable polarization is caused by a pulsation-driven dusty wind shell (see also Willson 2000; Höfner & Freytag 2022) that collides with a stellar wind bow shock, which is expected since V CVn is a runaway star. They argue that the shell is driven outwards from the star near maximum light, and because the shell is symmetric, the polarization is then at a minimum. However, the position angle will remain constant because of the constant presence of the asymmetric bow shock around the shell. As the shell expands and its density decreases, the polarization is set more by the near-constant density bow shock. This result is consistent with the apparent connection between the polarization amplitude and the tangential velocity observed for V CVn and its potential analogues, as described in Section 4.1. However, this model does not explain the apparent lead/lag time.

Additionally, instead of an asymmetry due to the presence of bow shocks, the wind may simply be asymmetric and variable. Simulations performed by Aronson et al. (2017) using non-spherical circumstellar shells that contain clumped material predicted significant net polarization signals. If the maximum polarization occurs near the minimum light then the wind, at that phase, could be most asymmetric, and at maximum light and minimum polarization, the wind would be most symmetric. It is worth noting that this argument is independent of wind density – since the polarization observed for V CVn is normalized – and is thus only concerned with changes in the symmetry of the wind as projected against the sky.

Asymmetric stellar winds are rare, but can be caused by rapid rotation as suggested for Be supergiants (e.g., Granada et al. 2010; Georgy et al. 2011), magnetic fields as seen in hot, massive stars with strong magnetic fields (e.g. Erba et al. 2021; Subramanian et al. 2022), or perhaps convection as suggested for massive evolved red supergiant stars (e.g., Kamiński 2019; López Ariste et al. 2022). There is no evidence that V CVn is a rapidly rotating star. However, given its evolved stage of evolution, its critical rotational velocity is small. Rotation might be important, and could be consistent with a small population of variable-polarization evolved stars. Furthermore, one would expect the rotation to be slow; however, it is possible there were dynamic events between the progenitors of these stars, and a companion spun up the progenitor (e.g., Staritsin 2022), while a supernova explosion or another dynamic event ejected the companion (Dorigo Jones et al. 2020). In that case, the progenitor would evolve into a runaway red giant star with rapid rotation. While this scenario may be possible, it is not obvious how to test this idea, and the proposed scenario should be a rare occurrence at best.

Strong magnetic fields ($> 1\text{kG}$) are not common among evolved stars (Grunhut et al. 2010); however, strong magnetic fields in hot stars are known to shape their stellar winds and make them asymmetric (e.g. ud-Doula & Owocki 2002). In hot (O- and B-type) stars, the magnetic field tends to be nearly dipolar, while in evolved stars the magnetic field is more tangled, and similar to that of the Sun. It is not clear that magnetic fields in this case can impact the wind structure in a meaningful manner, but the existence of a maser (Wolak et al. 2012) around V CVn

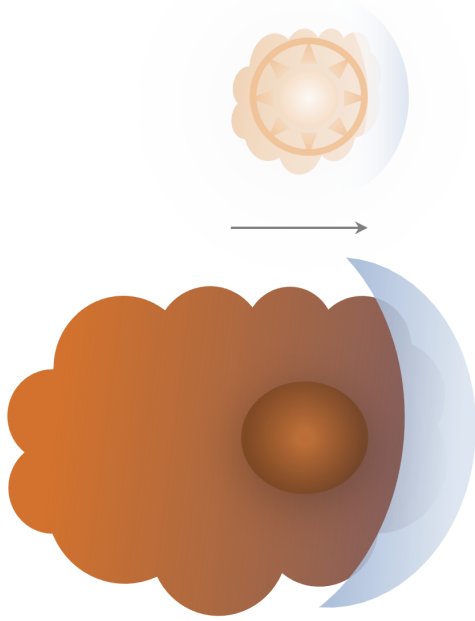


Fig. 7. A schematic representation of the interaction between the pulsating star and the bow shock. **Top:** at maximum brightness and minimum polarization, the dust is accelerated from the photosphere in a dense shell (circle) and the mass-loss rate is greatest. The star moves relative to the interstellar medium in the direction of the arrow. The wind shell is denser than the bow shock (light blue), and dominates the fraction of scattered light. **Bottom:** Around minimum light there is less radiative acceleration, and dust forms in the photosphere, while the mass-loss rate is much smaller. The shell formed at the previous flux maximum has expanded asymmetrically. The cloud-like structure of the dust envelope is supposed to show turbulence. A bow shock (blue) dominates the observed polarization, and is incorporated into the smaller density CSM. A lead/lag of the polarization and the light-curve can occur if convection causes the dust density in the line of sight and in the bow shock to develop differently.

implies that follow-up measurements would be a valuable test, and could be related to the observed polarization lead/lag.

Convection is unlikely to be the main source of polarizing photons in these red giant stars. Convection is not constant, and will create spots of some lifetime over different parts of a star that is not periodic. As such, the variable polarization should not be correlated with the brightness variation.

Although convection cannot be the main source of polarization, it is possible that the polarization lead/lag is caused by convection. It is known that, for pulsating Cepheids, convection can perturb their regular light curves to vary cycle-to-cycle (Derekas et al. 2012; Neilson & Ignace 2014; Derekas et al. 2017), and this is a potential cause of pulsation instability in variable red giant and supergiant stars. For V CVn, it is likely that convection and granulation make the times of maximum and minimum light unstable and variable in the same way. However, if the stellar wind is due to a dust shell being formed in the photosphere, then the wind is correlated more with the variability of the stellar radius and NOT the variability of the stellar luminosity. In Fig. 7, we have sketched the relationship between the pulsating star and the bow shock. We assume that with each pulsation cycle a different pattern of convection cells is created. In a pulsation cycle – where the dust is most dense first along the line of sight and only delayed in the direction of the bow shock – the brightness minimum occurs before the polarization maximum, and the po-

larization curve lags behind the brightness curve, as observed in pulsation cycle 1/2020, and vice-versa as in cycle 1/2021.

5. Conclusions

The new high-cadence photopolarimetry of V CVn presented here raises new questions about the nature of the polarization variability both of this star and other semi-regular variable stars. In particular, we find that the polarization maximum does not occur at the same time as light minimum, and that time will be a lead or a lag. This phenomenon is not naturally explained by the models proposed by either Neilson et al. (2014) or Safonov et al. (2019). Our investigation supports the hypothesis that the variable polarization is caused by a bow shock, and that the observed phase-shifts between polarization and light curves are caused by convective processes in the stellar photosphere. As such, we find that more high-cadence polarization measurements and simulations of V CVn-type stars would be important if we wish to understand the relationship between their stellar properties, their motions, and their circumstellar media.

Acknowledgements. The authors gratefully thank the Referee for the constructive comments and recommendations which helped to improve the paper. We acknowledge with thanks the variable star observations from the AAVSO International Database contributed by observers worldwide and used in this research. We thank Zenodo.org for hosting our data (<https://zenodo.org/record/7997101>). This work has made use of data from the European Space Agency (ESA) mission *Gaia* (<https://www.cosmos.esa.int/gaia>), processed by the *Gaia* Data Processing and Analysis Consortium (DPAC, <https://www.cosmos.esa.int/web/gaia/dpac/consortium>). Funding for the DPAC has been provided by national institutions, in particular the institutions participating in the *Gaia* Multilateral Agreement. MS is supported by an STFC consolidated grant number (ST/R000484/1) to LJM. HN acknowledges funding from NSERC.

References

- Aronson, E., Bladh, S., & Höfner, S. 2017, *A&A*, 603, A116
- Baug, T., Chandrasekhar, T., & Ganesh, S. 2014, *MNRAS*, 443, 3624
- Clarke, D. 2010, *Stellar Polarimetry*
- Davidson, J. W., Bjorkman, K. S., Hoffman, J. L., et al. 2014, *Journal of Astronomical Instrumentation*, 3, 1450009
- Derekas, A., Plachy, E., Molnár, L., et al. 2017, *MNRAS*, 464, 1553
- Derekas, A., Szabó, G. M., Berdnikov, L., et al. 2012, *MNRAS*, 425, 1312
- Dorigo Jones, J., Oey, M. S., Pagneot, K., Castro, N., & Moe, M. 2020, *ApJ*, 903, 43
- Dyck, H. M. & Jennings, M. C. 1971, *AJ*, 76, 431
- Erba, C., David-Uraz, A., Petit, V., et al. 2021, *MNRAS*, 506, 5373
- Gaia Collaboration. 2020, *VizieR Online Data Catalog*, I/350
- Georgy, C., Ekström, S., Granada, A., & Meynet, G. 2011, in *Active OB Stars: Structure, Evolution, Mass Loss, and Critical Limits*, ed. C. Neiner, G. Wade, G. Meynet, & G. Peters, Vol. 272, 640–641
- Gladders, M., Clarke, T., Burns, C., et al. 1998
- Granada, A., Jiménez, A., Curé, M., & Cidale, L. 2010, in *Revista Mexicana de Astronomía y Astrofísica Conference Series*, Vol. 38, *Revista Mexicana de Astronomía y Astrofísica Conference Series*, 60–60
- Grunhut, J. H., Wade, G. A., Hanes, D. A., & Alecian, E. 2010, *MNRAS*, 408, 2290
- Höfner, S. & Freytag, B. 2022, *arXiv e-prints*, arXiv:2204.09728
- Hsu, J. C. & Breger, M. 1982, *ApJ*, 262, 732
- Kamiński, T. 2019, *A&A*, 627, A114
- Kerschbaum, F. & Hron, J. 1992, *A&A*, 263, 97
- Kervella, P., Montargès, M., Lagarde, E., et al. 2015, *A&A*, 578, A77
- Kruszewski, A. & Coyne, G. V. 1976, *AJ*, 81, 641
- Kruszewski, A., Gehrels, T., & Serkowski, K. 1968, *AJ*, 73, 677
- Kudashkina, L. S. 2019, *Astrophysics*, 62, 556
- Lebzelter, T., Trabucchi, M., Mowlavi, N., et al. 2019, *A&A*, 631, A24
- López Ariste, A., Georgiev, S., Mathias, P., et al. 2022, *A&A*, 661, A91
- Magalhaes, A. M., Codina-Landaberry, S. J., Gneiding, C., & Coyne, G. V. 1986a, *A&A*, 154, 1
- Magalhaes, A. M., Coyne, G. V., & Benedetti, E. K. 1986b, *AJ*, 91, 919
- Magalhaes, A. M., Coyne, G. V., Codina-Landaberry, S. J., & Gneiding, C. 1986c, *A&A*, 154, 1
- Neilson, H. R. & Ignace, R. 2014, *A&A*, 563, L4

- Neilson, H. R., Ignace, R., Smith, B. J., Henson, G., & Adams, A. M. 2014, *A&A*, 568, A88
- Patat, F. & Romaniello, M. 2006, *Publications of the Astronomical Society of the Pacific*, 118, 146
- Ragland, S., Traub, W. A., Berger, J. P., et al. 2006, *ApJ*, 652, 650
- Reach, W. T., Koo, B.-C., & Heiles, C. 1994, *ApJ*, 429, 672
- Safonov, B. S., Dodin, A. V., Lamzin, S. A., & Rastorguev, A. S. 2019, *Astronomy Letters*, 45, 453
- Samus, N. N., Durlevich, O. V., & et al. 2004, *VizieR Online Data Catalog*, II/250
- Samus', N. N., Kazarovets, E. V., Durlevich, O. V., Kireeva, N. N., & Pastukhova, E. N. 2017, *Astronomy Reports*, 61, 80
- Schmidt, G. D., Elston, R., & Lupie, O. L. 1992, *AJ*, 104, 1563
- Serkowski, K. 1966, *Information Bulletin on Variable Stars*, 141, 1
- Serkowski, K. & Shawl, S. J. 2001, *AJ*, 122, 2017
- Shawl, S. J. 1975a, *AJ*, 80, 602
- Shawl, S. J. 1975b, *AJ*, 80, 595
- Shrestha, M., Neilson, H. R., Hoffman, J. L., Ignace, R., & Fullard, A. G. 2021, *MNRAS*, 500, 4319
- Staritsin, E. 2022, *arXiv e-prints*, arXiv:2209.00270
- Subramanian, S., Balsara, D. S., ud-Doula, A., & Gagné, M. 2022, *MNRAS*, 515, 237
- Trabucchi, M., Wood, P. R., Montalbán, J., et al. 2017, *ApJ*, 847, 139
- ud-Doula, A. & Owocki, S. P. 2002, *ApJ*, 576, 413
- Vartanyan, R. A. 1968, *Astrophysics*, 4, 51
- Wardle, J. F. C. & Kronberg, P. P. 1974, *ApJ*, 194, 249
- Willson, L. A. 2000, *ARA&A*, 38, 573
- Wolak, P., Szymczak, M., & Gérard, E. 2012, *A&A*, 537, A5

**Appendix A: The sample variable polarization
semi-regular variable stars.**

**Appendix B: The recorded photometric
measurements of V CVn**

Table A.1. V CVn type stars: semi-regular variables with significant variable polarization.

	V CVn	UZ Ari	AK Peg	RX Boo	Z UMa	L ₂ Pup
Spectral Type ¹	M4e-M6eIIIa	M8	M4-M8e	M6.5e-M8IIIe	M5IIIe	M5IIIe-M6IIIe
Galactic latitude (°)	70	-31	-43	69	57	-15
Period (d) ¹	194	163	194	162	195	-
$\Delta mag(V)$ ¹	2.0	0.8	1.6	2.7	3.2	3.6
Polarimetric data (yr)	1966 ² - 2022 ²	1972 ³ /2013 ⁴	1967 ⁵	1967 ⁵ , 1970 ⁶	1966 ⁷ , 1970 ⁶	1967 ⁸ -1982 ⁹
Polarization (%) ¹⁰	0.3 - 6.9	2 - 3.5	1.3 - 3.3	0.4 - 1.9	0.2 - 1.8	0 - 8
Position angle (°) ¹¹	80 - 120	126 - 132	21 - 50	40 - 153	8 - 132	165 - 180
Stability in ΔPA ¹²	yes	yes	unknown	unknown	unknown	yes
Distance (pc) ¹³	501	539	1329	156	296	56
μ (mas yr ⁻¹) ¹³	40	23	45	53	12	340
V_t (km s ⁻¹) ¹³	95	59	28	39	17	90
V_r (km s ⁻¹) ¹³	-47	n.a.	-4	-9	-53	53

¹ General catalog of variable stars Samus' et al. (2017)² Kruszewski et al. (1968), Dyck & Jennings (1971), Serkowski & Shawl (2001), Davidson et al. (2014), This study³ Kruszewski & Coyne (1976)⁴ Baug et al. (2014)⁵ R.A. Vartanyan, Intrinsic Polarization of Stellar Light From RX Boo, AB Cyg, Astrofizika, 1968⁶ Dyck & Jennings (1971)⁷ Serkowski (1966)⁸ Kruszewski et al. (1968)⁹ Magalhaes et al. (1986c)¹⁰ Range of measured polarization in V-Band as published in the above mentioned studies (RX Boo: intrinsic P)¹¹ Range of measured polarization angles in V-Band as published in the above mentioned studies¹² Yes, if position angle remains constant over the period of available polarization data¹³ Gaia Collaboration (2020)

Table B.1. Photopolarimetry journal of pulsation cycle 1/2020.

JD (d)	P_{cal} (debiased)	PA_{cal} ($^{\circ}$)	Q_{cal}	σ_Q	U_{cal}	σ_U	$mag(V)$	$\sigma_{mag(V)}$	Exp. (sec)	Ob.
2458947.3	0.0133	98.6	-0.0128	0.0018	-0.0039	0.0013	7.46	0.02	8	1
2458948.3	0.0149	106.1	-0.0126	0.0014	-0.0080	0.0013	7.43	0.02	8	1
2458950.3	0.0127	103.3	-0.0114	0.0010	-0.0057	0.0010	7.31	0.02	10	1
2458954.3	0.0127	102.8	-0.0117	0.0024	-0.0056	0.0027	7.13	0.02	10	1
2458956.3	0.0130	108.3	-0.0105	0.0011	-0.0078	0.0011	7.13	0.02	10	1
2458960.3	0.0097	100.7	-0.0091	0.0007	-0.0036	0.0008	7.35	0.02	10	1
2458961.3	0.0112	110.8	-0.0085	0.0014	-0.0075	0.0013	7.16	0.02	10	1
2458962.3	0.0124	106.0	-0.0105	0.0007	-0.0066	0.0010	7.2	0.02	10	1
2458963.3	0.0133	103.8	-0.0119	0.0008	-0.0062	0.0008	7.18	0.02	10	1
2458966.3	0.0140	107.5	-0.0115	0.0015	-0.0081	0.0010	7.19	0.02	10	1
2458967.3	0.0136	109.9	-0.0105	0.0012	-0.0088	0.0010	7.26	0.02	10	1
2458969.3	0.0120	108.8	-0.0095	0.0007	-0.0073	0.0015	7.2	0.02	10	1
2458976.3	0.0123	107.3	-0.0102	0.0008	-0.0070	0.0009	7.08	0.02	10	1
2458977.3	0.0137	106.3	-0.0116	0.0008	-0.0074	0.0012	7.3	0.02	10	1
2458980.3	0.0135	111.2	-0.0101	0.0009	-0.0092	0.0020	7.32	0.05	10	1
2458987.3	0.0110	102.5	-0.0100	0.0010	-0.0047	0.0012	7.33	0.02	10	1
2458988.3	0.0105	106.5	-0.0089	0.002	-0.0058	0.0009	7.28	0.02	10	1
2458990.3	0.0119	105.2	-0.0103	0.0009	-0.006	0.0012	7.34	0.02	10	1
2458991.3	0.0121	105.9	-0.0104	0.0009	-0.0064	0.0012	7.35	0.02	10	1
2458996.3	0.0097	96.0	-0.0095	0.0012	-0.002	0.0012	7.34	0.02	10	1
2458997.3	0.0100	103.0	-0.009	0.0011	-0.0044	0.0014	7.51	0.02	10	1
2458999.4	0.0085	102.1	-0.008	0.0019	-0.0036	0.0012	7.59	0.02	10	1
2459002.4	0.0133	100.5	-0.0125	0.0012	-0.0048	0.0009	7.52	0.02	10	1
2459003.4	0.0119	97.8	-0.0115	0.0009	-0.0032	0.0013	7.55	0.02	10	1
2459013.4	0.0155	101.2	-0.0144	0.0011	-0.0059	0.0014	7.68	0.02	10	1
2459019.4	0.0144	105.1	-0.0126	0.0028	-0.0073	0.0014	7.63	0.02	10	1
2459024.4	0.0175	107.0	-0.0146	0.0013	-0.0098	0.0012	7.57	0.02	10	1
2459031.4	0.0161	110.3	-0.0122	0.0008	-0.0105	0.001	7.27	0.02	10	1
2459034.4	0.0170	109.8	-0.0131	0.001	-0.0108	0.001	7.22	0.02	10	1
2459035.4	0.0151	110.6	-0.0114	0.0011	-0.01	0.0013	7.23	0.02	10	1
2459036.4	0.0148	109.1	-0.0116	0.0011	-0.0092	0.0011	7.18	0.02	10	1
2459038.4	0.0122	109.8	-0.0094	0.0007	-0.0078	0.001	7.06	0.02	10	1
2459040.4	0.0147	110.1	-0.0112	0.001	-0.0095	0.0009	6.98	0.02	10	1
2459043.4	0.0130	111.6	-0.0095	0.0011	-0.0089	0.001	7.04	0.02	10	1
2459050.4	0.0114	112.0	-0.0083	0.0012	-0.008	0.0025	6.8	0.05	10	1
2459051.4	0.0089	117.7	-0.0051	0.001	-0.0074	0.0011	6.79	0.02	10	1
2459054.4	0.0094	110.8	-0.0071	0.0012	-0.0063	0.0014	6.75	0.02	10	1
2459056.4	0.0083	108.5	-0.0068	0.0016	-0.0051	0.0016	6.74	0.02	10	1
2459058.4	0.0073	102.5	-0.0067	0.0011	-0.0031	0.0009	6.63	0.02	10	1
2459060.4	0.0046	102.7	-0.0042	0.0009	-0.002	0.001	6.58	0.02	10	1
2459061.4	0.0053	101.0	-0.005	0.0006	-0.002	0.0013	6.63	0.02	10	1
2459062.3	0.0034	101.1	-0.0034	0.0011	-0.0014	0.0009	6.61	0.02	10	1
2459067.3	0.0064	93.7	-0.0064	0.001	-0.0008	0.001	6.74	0.02	10	1
2459069.3	0.0026	98.8	-0.0029	0.0015	-0.0009	0.0012	6.67	0.02	10	1
2459072.3	0.0034	83.3	-0.0036	0.0015	0.0009	0.0016	6.65	0.02	10	1
2459077.3	0.0047	78.9	-0.0045	0.0011	0.0018	0.0016	6.77	0.02	10	1
2459081.3	0.0071	74.4	-0.0062	0.0013	0.0037	0.0017	6.96	0.02	10	1
2459110.4	0.0079	76.8	-0.0071	0.0008	-0.0035	0.0011	7.2	0.02	20	2
2459113.4	0.0103	82.4	-0.0101	0.0011	-0.0027	0.0009	7.2	0.02	20	2
2459118.4	0.0093	82.5	-0.009	0.0002	-0.0024	0.0007	7.17	0.02	30	2
2459119.4	0.0082	81.9	-0.0079	0.0003	-0.0023	0.0012	7.17	0.02	30	2

Table B.2. Journal of measurements from 2021, part 1.

JD (d)	P_{cal} (debiased)	PA_{cal} ($^{\circ}$)	Q_{cal}	σ_Q	U_{cal}	σ_U	$mag(V)$	$\sigma_{mag(V)}$	$Exp.$ (sec)	$Ob.$
2459266.4	0.0112	96.5	-0.011	0.0014	-0.0025	0.0015	6.68	0.02	7	1
2459267.4	0.0121	95.0	-0.0121	0.0017	-0.0021	0.0022	6.7	0.02	10	1
2459268.4	0.0122	87.8	-0.0123	0.0019	0.001	0.0024	6.77	0.02	7	1
2459269.4	0.0126	91.5	-0.0127	0.0017	-0.0007	0.0021	6.83	0.02	10	1
2459270.4	0.0106	87.8	-0.0106	0.0014	0.0008	0.0016	6.83	0.02	10	1
2459271.4	0.0097	87.1	-0.0096	0.0014	0.0010	0.0015	6.87	0.02	7	1
2459273.3	0.0133	94.0	-0.0133	0.0013	-0.0018	0.0015	6.91	0.02	7	1
2459274.3	0.0147	86.4	-0.0149	0.0026	0.0019	0.0027	6.87	0.02	7	1
2459275.3	0.0108	86.3	-0.0109	0.0015	0.0014	0.001	6.92	0.02	10	1
2459276.3	0.0103	77.1	-0.0094	0.0015	0.0046	0.0015	6.9	0.02	10	1
2459276.4	0.0100	73.4	-0.0084	0.0008	0.0055	0.0007	6.93	0.02	10	2
2459279.3	0.0114	64.8	-0.0073	0.0009	0.0088	0.0011	6.97	0.02	10	2
2459280.3	0.0101	64.3	-0.0068	0.0041	0.0086	0.0045	6.74	0.02	10	1
2459282.3	0.0112	80.5	-0.0106	0.0012	0.0037	0.0015	7.02	0.02	10	2
2459287.4	0.0110	79.8	-0.0104	0.0012	0.0039	0.0015	7.03	0.02	10	2
2459290.4	0.0114	80.6	-0.0108	0.0009	0.0037	0.0009	7.04	0.02	12	2
2459292.4	0.0109	81.2	-0.0104	0.0005	0.0033	0.0007	7.08	0.02	10	2
2459295.4	0.0116	85.7	-0.0115	0.0005	0.0017	0.0008	7.08	0.02	10	2
2459297.3	0.0125	92.3	-0.0124	0.0004	-0.001	0.0016	7.1	0.02	10	1
2459298.3	0.0107	89.7	-0.0107	0.0005	0.0001	0.0006	7.11	0.02	10	1
2459303.3	0.0125	95.1	-0.0123	0.0006	-0.0022	0.0007	7.35	0.02	10	1
2459304.3	0.0134	96.6	-0.013	0.0006	-0.003	0.0006	7.26	0.02	10	1
2459305.4	0.0133	92.3	-0.0133	0.001	-0.001	0.0007	7.17	0.02	5	1
2459307.3	0.0149	98.3	-0.0143	0.0003	-0.0043	0.0007	7.23	0.02	5	1
2459308.4	0.0161	94.4	-0.0159	0.0006	-0.0025	0.0007	7.2	0.02	10	2
2459309.3	0.0168	101.1	-0.0156	0.0008	-0.0064	0.0007	7.2	0.02	5	1
2459313.3	0.0203	104.0	-0.018	0.0006	-0.0096	0.0007	7.35	0.02	5	1
2459314.4	0.0232	103.8	-0.0206	0.0006	-0.0108	0.0009	-	-	5	1
2459316.3	0.0249	105.8	-0.0212	0.0003	-0.0131	0.0007	7.25	0.02	5	1
2459317.4	0.0234	99.6	-0.0221	0.0005	-0.0077	0.0007	7.25	0.02	10	2
2459319.4	0.0248	99.9	-0.0233	0.0005	-0.0084	0.0007	7.28	0.02	11	2
2459320.4	0.0241	100.7	-0.0225	0.0006	-0.0087	0.0007	7.29	0.02	11	2
2459321.3	0.0242	106.5	-0.0203	0.0007	-0.0132	0.0007	7.36	0.02	5	1
2459325.3	0.0258	108.7	-0.0205	0.0011	-0.0157	0.0013	7.44	0.02	5	1
2459326.4	0.0272	103.8	-0.0241	0.0007	-0.0126	0.0009	7.4	0.02	10	2
2459327.3	0.0241	108.3	-0.0194	0.0006	-0.0144	0.0007	7.43	0.02	5	1
2459328.3	0.0249	109.5	-0.0193	0.0007	-0.0157	0.0007	7.48	0.02	5	1
2459329.3	0.0255	110.1	-0.0195	0.0015	-0.0165	0.0009	7.6	0.02	5	1
2459330.3	0.0255	110.2	-0.0194	0.0008	-0.0165	0.0008	7.55	0.02	5	1
2459331.3	0.0263	108.9	-0.0208	0.0007	-0.0161	0.0007	7.54	0.02	5	1
2459332.3	0.0253	109.6	-0.0196	0.0008	-0.016	0.0007	7.55	0.02	5	1
2459338.3	0.0300	110.4	-0.0227	0.001	-0.0197	0.0007	7.78	0.02	5	1
2459340.4	0.0235	110.6	-0.0177	0.0006	-0.0155	0.0009	-	-	5	1
2459340.4	0.0252	105.4	-0.0217	0.0009	-0.0129	0.0009	7.74	0.02	15	2
2459340.5	0.0258	106.3	-0.0221	0.0011	-0.0134	0.0009	7.74	0.02	15	2
2459342.5	0.0257	106.3	-0.0217	0.0009	-0.0138	0.001	7.78	0.02	15	2
2459342.3	0.0257	109.5	-0.0199	0.0005	-0.0162	0.0007	7.75	0.02	5	1
2459343.4	0.0212	112.9	-0.0148	0.0006	-0.0152	0.0008	7.79	0.02	5	1
2459353.4	0.0190	104.6	-0.0167	0.0028	-0.0094	0.0008	7.92	0.02	15	2
2459354.3	0.0212	114.0	-0.0143	0.0028	-0.0159	0.0011	7.99	0.02	5	1
2459364.4	0.0117	109.7	-0.0091	0.0005	-0.0074	0.0011	7.72	0.02	5	1
2459365.4	0.0140	117.6	-0.008	0.0006	-0.0115	0.0007	7.57	0.02	5	1

Table B.3. Journal of measurements from 2021, part 2.

JD (d)	P_{cal} (debiased)	PA_{cal} ($^{\circ}$)	Q_{cal}	σ_Q	U_{cal}	σ_U	$mag(V)$	$\sigma_{mag(V)}$	$Exp.$ (sec)	$Ob.$
2459367.4	0.0120	111.6	-0.0088	0.0006	-0.0082	0.0008	7.57	0.02	5	1
2459370.4	0.0118	106.5	-0.0099	0.0008	-0.0064	0.0010	7.66	0.02	5	1
2459374.4	0.0104	106.3	-0.0088	0.0011	-0.0056	0.0012	7.38	0.02	5	1
2459377.4	0.0116	104.4	-0.0102	0.0006	-0.0056	0.0009	7.51	0.02	5	1
2459379.4	0.0111	102.1	-0.0101	0.0006	-0.0046	0.0008	7.16	0.02	5	1
2459380.4	0.0101	111.6	-0.0088	0.002	-0.0053	0.0007	7.1	0.02	5	1
2459381.4	0.0120	102.0	-0.011	0.0007	-0.0049	0.0009	7.15	0.02	5	1
2459383.4	0.0112	99.8	-0.0105	0.0006	-0.0038	0.0007	7.18	0.02	5	1
2459389.4	0.0123	100.8	-0.0115	0.0006	-0.0045	0.0008	7.09	0.02	5	1
2459392.4	0.0135	98.4	-0.013	0.0006	-0.0039	0.0008	6.88	0.02	5	1
2459401.4	0.0120	98.3	-0.0115	0.001	-0.0035	0.0009	7.07	0.02	5	1
2459405.4	0.0128	99.2	-0.0122	0.0007	-0.004	0.0011	7.35	0.02	5	1
2459407.3	0.0140	98.7	-0.0134	0.001	-0.0042	0.0007	7.31	0.02	5	1
2459412.3	0.0133	97.7	-0.0129	0.0013	-0.0035	0.0012	7.31	0.02	5	1
2459412.5	0.0133	93.6	-0.0132	0.0007	-0.0017	0.0008	7.35	0.02	10	2
2459413.5	0.0132	93.3	-0.0131	0.0008	-0.0015	0.0009	7.36	0.02	10	2
2459414.4	0.0145	99.3	-0.0138	0.0007	-0.0046	0.0014	7.34	0.02	5	1
2459415.3	0.0112	99.1	-0.0107	0.0008	-0.0035	0.0009	7.44	0.02	5	1
2459416.3	0.0112	96.6	-0.0109	0.0009	-0.0026	0.0009	7.3	0.02	5	1
2459416.5	0.0128	92.2	-0.0128	0.0006	-0.001	0.0008	7.31	0.02	10	2
2459417.3	0.0108	95.6	-0.0107	0.001	-0.0021	0.0008	7.25	0.02	5	1
2459417.6	0.0107	91.3	-0.0108	0.0013	-0.0003	0.0013	7.33	0.02	10	2
2459418.3	0.0111	95.6	-0.011	0.0012	-0.0022	0.0013	7.3	0.02	5	1
2459419.3	0.0086	93.2	-0.0086	0.0013	-0.001	0.0012	7.26	0.02	5	1
2459425.3	0.0078	89.2	-0.0078	0.0006	0.0002	0.0009	7.16	0.02	5	1
2459429.5	0.0063	85.9	-0.0063	0.0005	0.0009	0.0007	6.98	0.02	12	2
2459436.3	0.0043	66.9	-0.003	0.001	0.0032	0.001	6.76	0.02	5	1
2459437.3	0.0037	63.0	-0.0023	0.0013	0.0032	0.0012	6.69	0.02	5	1
2459439.3	0.0033	69.4	-0.0026	0.001	0.0023	0.0011	6.71	0.02	2	1
2459440.3	0.0039	67.3	-0.0029	0.0014	0.003	0.001	6.77	0.02	3	1
2459441.3	0.0046	67.5	-0.0033	0.0007	0.0033	0.0011	6.87	0.02	3	1
2459453.4	0.0052	81.6	-0.005	0.0005	0.0015	0.0007	6.77	0.02	12	2
2459454.4	0.0048	79.9	-0.0045	0.0005	0.0017	0.0007	6.8	0.02	12	2
2459459.4	0.0046	86.0	-0.0046	0.0005	0.0006	0.0006	6.86	0.02	15	2
2459465.4	0.0075	84.1	-0.0074	0.0005	0.0015	0.0006	6.93	0.02	15	2
2459477.4	0.0080	100.6	-0.0075	0.0004	-0.0029	0.0006	7.1	0.02	15	2
2459487.4	0.0097	99.8	-0.0092	0.001	-0.0032	0.0013	7.23	0.02	15	2

Table B.4. Journal of measurements from 2022, part 1.

JD (d)	P_{cal} (debiased)	PA_{cal} ($^{\circ}$)	Q_{cal}	σ_Q	U_{cal}	σ_U	$mag(V)$	$\sigma_{mag(V)}$	$Exp.$ (sec)	$Ob.$
2459609.4	0.0140	91.7	-0.014	0.0005	-0.0008	0.0006	7.36	0.02	15	2
2459617.4	0.0120	91.4	-0.012	0.0004	-0.0006	0.0006	7.01	0.02	15	2
2459619.4	0.0103	93.0	-0.0103	0.0003	-0.0011	0.0006	6.89	0.02	5	1
2459620.4	0.0092	89.6	-0.0092	0.0004	0.0001	0.0007	6.82	0.02	5	1
2459622.4	0.0099	90.7	-0.01	0.0008	-0.0002	0.001	6.79	0.02	5	1
2459623.4	0.0089	78.7	-0.0083	0.0004	0.0034	0.0007	6.78	0.02	5	1
2459624.3	0.0088	90.0	-0.0088	0.0003	0.0000	0.0006	6.67	0.02	5	1
2459625.4	0.0090	91.2	-0.009	0.0004	-0.0004	0.0006	6.68	0.02	15	2
2459626.4	0.0102	90.6	-0.0102	0.0005	-0.0002	0.0007	6.61	0.02	5	1
2459630.4	0.0090	94.1	-0.0089	0.0003	-0.0013	0.0006	6.58	0.02	5	1
2459634.4	0.0080	90.2	-0.008	0.0004	0.0000	0.0007	6.57	0.02	5	1
2459637.4	0.0078	93.3	-0.0077	0.0004	-0.0009	0.0007	6.52	0.02	5	1
2459637.4	0.0092	95.3	-0.009	0.0004	-0.0017	0.0006	6.54	0.02	15	2
2459639.4	0.0076	90.9	-0.0077	0.0005	-0.0002	0.0007	6.63	0.02	5	1
2459640.3	0.0080	93.1	-0.008	0.0003	-0.0009	0.0006	6.62	0.02	5	1
2459640.4	0.0074	90.7	-0.0074	0.0004	-0.0002	0.0006	6.56	0.02	14	2
2459642.4	0.0064	88.8	-0.0065	0.0003	0.0003	0.0006	6.57	0.02	5	1
2459644.4	0.0071	93.0	-0.0071	0.0004	-0.0007	0.0006	6.61	0.02	15	2
2459646.3	0.0076	99.9	-0.0072	0.0004	-0.0026	0.0006	6.61	0.02	13	2
2459653.5	0.0093	94.0	-0.0092	0.0004	-0.0013	0.0006	6.68	0.02	10	2
2459657.4	0.0067	80.4	-0.0063	0.0004	0.0022	0.0006	6.76	0.02	10	2
2459658.4	0.0083	92.5	-0.0083	0.0004	-0.0007	0.0006	6.77	0.02	10	2
2459659.4	0.0085	93.6	-0.0084	0.0005	-0.0011	0.0006	6.79	0.02	15	2
2459661.4	0.0100	96.0	-0.0098	0.0005	-0.0021	0.0007	6.83	0.02	15	2
2459664.4	0.0101	96.9	-0.0098	0.0004	-0.0024	0.0006	6.92	0.02	13	2
2459666.4	0.0090	89.1	-0.009	0.0005	0.0003	0.0006	6.95	0.02	11	2
2459669.4	0.0128	91.2	-0.0128	0.0005	-0.0005	0.0007	7.01	0.02	11	2
2459679.3	0.0171	98.2	-0.0164	0.0021	-0.0048	0.0021	7.24	0.02	5	1
2459681.3	0.0172	101.3	-0.0159	0.0003	-0.0066	0.0007	7.29	0.02	5	1
2459683.3	0.0171	98.4	-0.0164	0.0004	-0.0049	0.0007	7.23	0.02	5	1
2459684.3	0.0158	94.5	-0.0157	0.0005	-0.0025	0.0008	7.28	0.02	5	1
2459686.3	0.0180	103.5	-0.0161	0.0006	-0.0082	0.0008	7.24	0.02	5	1
2459687.3	0.0186	105.1	-0.0161	0.0005	-0.0094	0.0007	7.21	0.02	5	1
2459688.4	0.0182	105.7	-0.0156	0.0005	-0.0095	0.0007	7.24	0.02	5	1
2459691.3	0.0184	110.7	-0.0138	0.0016	-0.0122	0.0017	7.27	0.02	5	1
2459692.4	0.0190	105.6	-0.0163	0.0004	-0.0098	0.0006	7.22	0.02	12	2
2459697.4	0.0166	107.9	-0.0135	0.0004	-0.0097	0.0007	7.2	0.02	12	2
2459698.4	0.0157	115.2	-0.0101	0.0021	-0.0122	0.0022	7.2	0.02	5	1
2459709.4	0.0107	114.1	-0.0071	0.0005	-0.008	0.0008	7.16	0.02	5	1
2459715.3	0.0104	109.5	-0.0081	0.0006	-0.0065	0.0008	7.06	0.02	5	1
2459717.3	0.0095	108.3	-0.0076	0.0004	-0.0057	0.0007	7.22	0.02	5	1
2459718.3	0.0092	107.4	-0.0076	0.0005	-0.0053	0.0007	7.29	0.02	5	1
2459721.3	0.0082	103.2	-0.0073	0.0006	-0.0036	0.0008	7.37	0.02	5	1
2459725.3	0.0117	106.8	-0.0098	0.0007	-0.0065	0.0009	7.41	0.02	5	1

Table B.5. Journal of measurements from 2022, part 2.

JD (d)	P_{cal} (debiased)	PA_{cal} ($^{\circ}$)	Q_{cal}	σ_Q	U_{cal}	σ_U	$mag(V)$	$\sigma_{mag(V)}$	Exp. (sec)	Ob.
2459726.4	0.0128	109.5	-0.01	0.0007	-0.0081	0.0009	7.45	0.02	5	1
2459730.4	0.0124	104.2	-0.011	0.0005	-0.0059	0.0008	7.54	0.02	5	1
2459733.4	0.0137	102.8	-0.0124	0.0007	-0.006	0.0009	7.59	0.02	5	1
2459741.4	0.0175	90.0	-0.0175	0.0005	0.0000	0.0007	7.71	0.02	5	1
2459742.4	0.0176	101.2	-0.0163	0.0007	-0.0067	0.0009	7.71	0.02	5	1
2459743.4	0.0183	99.9	-0.0172	0.0007	-0.0062	0.0009	7.79	0.02	5	1
2459745.4	0.0188	99.1	-0.0179	0.001	-0.0059	0.0011	7.74	0.02	5	1
2459750.4	0.0199	93.3	-0.0198	0.0009	-0.0023	0.001	7.76	0.02	5	1
2459760.3	0.0198	97.8	-0.0191	0.0012	-0.0053	0.0013	7.63	0.02	5	1
2459762.4	0.0153	90.5	-0.0153	0.0006	-0.0003	0.0008	7.58	0.02	5	1
2459763.4	0.0228	94.4	-0.0226	0.0007	-0.0035	0.0009	7.58	0.02	5	1
2459764.4	0.0150	84.2	-0.0147	0.0009	0.003	0.001	7.47	0.02	5	1
2459766.4	0.0193	92.5	-0.0193	0.0006	-0.0017	0.0008	7.53	0.02	5	1
2459769.4	0.0188	94.8	-0.0186	0.0005	-0.0031	0.0007	7.52	0.02	5	1
2459771.4	0.0172	90.0	-0.0172	0.0002	0.0000	0.0006	7.54	0.02	5	1
2459773.3	0.0189	93.7	-0.0188	0.0017	-0.0025	0.0018	7.52	0.02	5	1
2459777.3	0.0177	91.8	-0.0177	0.0009	-0.0011	0.0011	7.46	0.02	5	1
2459778.3	0.0182	93.4	-0.0181	0.0006	-0.0022	0.0008	7.45	0.02	5	1
2459780.3	0.0170	94.8	-0.0168	0.0005	-0.0028	0.0007	7.43	0.02	5	1
2459782.3	0.0181	93.3	-0.018	0.001	-0.0021	0.0012	7.38	0.02	5	1
2459785.3	0.0182	95.7	-0.0179	0.0007	-0.0036	0.0009	7.32	0.02	5	1
2459787.3	0.0155	93.5	-0.0154	0.0013	-0.0019	0.0014	7.28	0.02	5	1
2459794.3	0.0157	96.7	-0.0153	0.0005	-0.0036	0.0007	7.19	0.02	5	1
2459795.3	0.0182	100.6	-0.017	0.0005	-0.0066	0.0008	7.2	0.02	5	1
2459796.3	0.0178	98.5	-0.0171	0.0006	-0.0052	0.0008	7.16	0.02	5	1
2459800.3	0.0175	99.2	-0.0166	0.0008	-0.0055	0.001	7.2	0.02	5	1
2459801.3	0.0148	97.0	-0.0144	0.0007	-0.0036	0.0009	7.21	0.02	5	1
2459802.3	0.0159	99.0	-0.0151	0.0007	-0.0049	0.0009	7.28	0.02	5	1
2459802.5	0.0186	94.2	-0.0184	0.0004	-0.0027	0.0006	7.22	0.02	12	2
2459803.4	0.0161	94.5	-0.0159	0.0006	-0.0024	0.0007	7.22	0.02	11	2
2459808.3	0.0164	97.6	-0.0158	0.0008	-0.0043	0.0009	7.25	0.02	5	1
2459810.5	0.0175	95.6	-0.0172	0.0007	-0.0034	0.0007	7.25	0.02	14	2
2459815.4	0.0160	95.9	-0.0157	0.0009	-0.0033	0.001	7.2	0.02	14	2
2459824.4	0.0164	100.6	-0.0153	0.0005	-0.0059	0.0006	7.17	0.02	13	2
2459833.4	0.0145	97.1	-0.0141	0.0006	-0.0036	0.0008	7.21	0.02	15	2
2459837.4	0.0112	95.4	-0.011	0.0005	-0.0021	0.0007	7.17	0.02	15	2
2459845.3	0.0107	100	-0.0101	0.0005	-0.0037	0.0007	7.12	0.02	15	2
2459847.3	0.0116	97.8	-0.0112	0.0004	-0.0031	0.0007	7.12	0.02	15	2
2459849.3	0.0132	95.2	-0.013	0.0005	-0.0024	0.0006	7.1	0.02	15	2
2459850.3	0.0128	103.7	-0.0114	0.0005	-0.0059	0.0006	7.08	0.02	15	2
2459865.4	0.0173	111.5	-0.0126	0.0004	-0.0118	0.0007	6.98	0.02	15	2
2459867.3	0.0169	111.9	-0.0122	0.0005	-0.0117	0.0007	7.00	0.02	15	2
2459887.7	0.0184	124.0	-0.0069	0.0006	-0.0171	0.0008	7.33	0.02	15	2